



This is the accepted manuscript made available via CHORUS. The article has been published as:

## Accurate equation of state of math

$\text{H}_2/\text{He}$  binary mixtures up to 5.4 GPa

Charlie M. Zoller, Muhtar Ahart, Sakun Duwal, Raymond C. Clay, III, Christopher T. Seagle, Young Jay Ryu, Sergey Tkachev, Stella Chariton, Vitali Prakapenka, and Russell J. Hemley

Phys. Rev. B **108**, 224112 — Published 26 December 2023

DOI: [10.1103/PhysRevB.108.224112](https://doi.org/10.1103/PhysRevB.108.224112)

# Accurate Equation of State of H<sub>2</sub>-He Binary Mixtures up to 5.4 GPa

Charlie M. Zoller<sup>1</sup>, Muhtar Ahart<sup>1</sup>, Sakun Duwal<sup>2</sup>, Raymond Clay<sup>2</sup>, Christopher T. Seagle<sup>2</sup>, Young Jay Ryu<sup>3</sup>, Sergey Tkachev<sup>3\*</sup>, Stella Chariton<sup>3</sup>, Vitali Prakapenka<sup>3</sup>, and Russell Hemley<sup>1,4,5</sup>

<sup>1</sup> *Department of Physics, University of Illinois Chicago, Chicago, IL 60607*

<sup>2</sup> *Sandia National Laboratories, Albuquerque, NM 87125*

<sup>3</sup> *GSECARS, University of Chicago, Argonne National Laboratory, Argonne, IL 60439*

<sup>4</sup> *Department of Chemistry, University of Illinois Chicago, Chicago, IL 60607*

<sup>5</sup> *Department of Earth and Environmental Sciences, University of Illinois Chicago, Chicago, IL 60607*

Brillouin scattering spectroscopy has been used to obtain an accurate (<1%)  $\rho$ - $P$  equation of state (EOS) of 1:1 and 9:1 H<sub>2</sub>-He molar mixtures from 0.5 to 5.4 GPa at 296 K. Our calculated equations of state indicate close agreement with the experimental data right to the freezing pressure of hydrogen at 5.4 GPa. The measured velocities agree on average, within 0.5%, of an ideal mixing model. The  $\rho$ - $P$  EOS presented have a standard deviation of under 0.3% from the measured densities and under 1% deviation from ideal mixing. A detailed discussion of the accuracy, precision, and sources of error in the measurement and analyses of our equations of state is presented.

## I. Introduction

The properties of fluid hydrogen-helium (H<sub>2</sub>-He) mixtures as a function of density are of broad importance in condensed matter physics and chemistry<sup>1</sup> and planetary science<sup>2</sup>. As the most abundant and electronically simplest elements with strong nuclear quantum properties, hydrogen and helium represent ideal candidates for studying the intermolecular and interatomic interactions in mixtures under pressure. Continued developments in dynamic compression techniques have greatly increased the pressure-temperature ( $P$ - $T$ ) ranges over which H<sub>2</sub> and He have been investigated in the laboratory.<sup>3-17</sup> Specifically, studies of H<sub>2</sub><sup>3-5</sup>, D<sub>2</sub><sup>5-8</sup>, He<sup>9-13</sup>, and H<sub>2</sub>-He<sup>14-16</sup> mixtures have been conducted using various combinations of shock and ramp compression with cryogenic or precompressed samples. Dynamic compression experiments on precompressed samples require a highly accurate equation of state (EOS) to set the initial conditions of the measurement. This technique enables the measurement of higher final density states<sup>18</sup>. For hydrogen and helium mixtures, such an EOS is not yet in hand, yet it is essential for the analysis of recent dynamic compression measurements to megabar (>100 GPa) pressures.

A method to increase the final density state in dynamic compression involves precompressing the sample<sup>18</sup>. The effect of precompressing samples is easily seen in the Hugoniot EOS.

$$E - E_0 = \frac{1}{2}M(P + P_0) \left( \frac{1}{\rho} - \frac{1}{\rho_0} \right) \quad (1)$$

The accuracy of shock state variables are highly dependent on the accuracy of precompression; an error of 2-3% of the initial density state can propagate to uncertainty in the final shock state of 7-10%<sup>15</sup>.

There is a significant body of literature on the thermodynamic properties of fluid H<sub>2</sub> from fractions of a bar to its ambient temperature freezing pressure and temperatures to 1000 K<sup>19</sup>.

Thermodynamic data for helium extends from fractions of a bar to its ambient temperature freezing pressure. Lower pressure studies on helium have reached 1500 K<sup>20</sup>. There have also been studies in the 100 MPa to GPa ranges using ultrasonic<sup>21</sup> and Brillouin spectroscopy for sound velocity measurements<sup>22-26</sup>, and volumetric measurements<sup>27</sup>. Equations of state have been developed for helium from ambient pressure to helium freezing (11.6 GPa) using Brillouin<sup>28-30</sup> spectroscopy, ultrasonic spectroscopy<sup>21,26,27</sup>, and volumetric measurements<sup>27</sup>. The density of a material is directly related to the measured sound velocity.

$$\left(\frac{\partial \rho}{\partial P}\right)_S = \frac{1}{U_l^2} \quad (2)$$

Through integration, one obtains the  $\rho$ -P EOS.

$$\rho - \rho_0 = \int_{P_0}^P dP \frac{\gamma}{U_l^2} \quad (3)$$

Where  $\rho_0$  is a reference density,  $\gamma = \frac{c_p}{c_v}$ , and  $U_l$  is the longitudinal sound velocity of the material.

Hydrogen and helium are supercritical fluids over the range of pressures studied here, with the critical pressure  $P^*$  and temperature  $T^*$  of 1.3 MPa and 33.2 K and 227 kPa and 5.3 K<sup>31</sup> for hydrogen and helium, respectively. Assuming no phase separation (changing miscibility), the supercritical fluid nature of the system results in a continuous  $\rho$ -P relation without volume discontinuities from condensation.

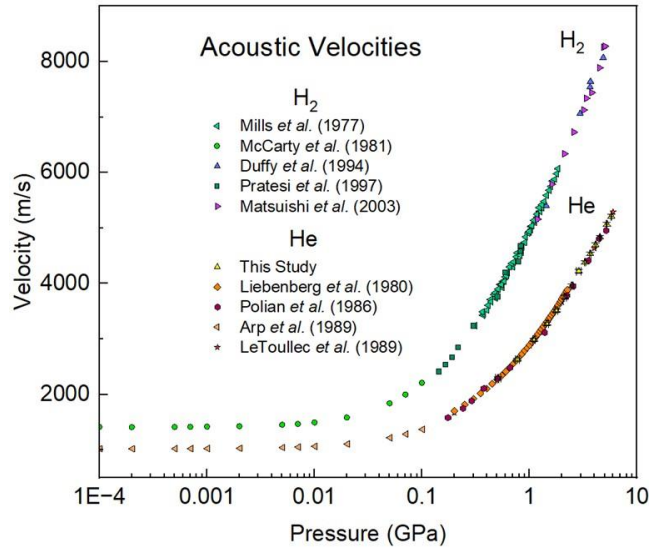


**FIG. 1.**  $H_2$ <sup>21-23, 32, 33</sup> and  $He$ <sup>20, 28, 30, 34</sup>  $U_l$ -P EOS from ambient to freezing pressures at 293-300 K.

There is currently no experimental fluid  $H_2$ -He  $\rho$ -P EOS; therefore, the ideality of mixing is unknown. An ideal mixture will have its physical properties scale in proportion to its constituents. Interaction and size effects will affect the (non)ideality of the mixture, so direct measurement is necessary to determine the effect non-ideal mixing will have on the EOS. The calculated energy of interaction indicates that the interaction between  $H_2$  and He is significantly less than the self-interaction of their pure constituents<sup>35</sup> and  $H_2$  and He appear to have ~1%

excess volume of mixing up to 1 GPa at 100 K<sup>36</sup>; the excess volume at 300 K will be less as thermal energy will increasingly dominate repulsive H<sub>2</sub> and He interactions with increasing temperature. It will also be important to note possible discontinuities due to demixing of H<sub>2</sub> and He, meaning possible non-idealities at certain mixing ratios resulting in a miscibility gap. Several studies indicate possible fluid-fluid separation near the freezing of pure hydrogen<sup>37-39</sup>. If non-ideal mixing occurs anywhere in H<sub>2</sub>:He mixtures, it will be near the fluid-fluid demixing pressures and compositions.

This study seeks to develop an accurate EOS to address possible non-ideality of mixing in the  $\rho$ - $P$  EOS using measurements of the sound velocity of the mixtures by Brillouin scattering. Armed with an accurate EOS, the initial ( $\rho_0, P_0$ ) precompression measurements allow an accurate calculation of the final ( $\rho, P$ ) dynamic compression state of the system.

## II. Experimental Methods

Our samples were prepared inside BX-90 diamond anvil cells (DACs) with 600  $\mu\text{m}$  culets. The DACs were gas loaded with ultra-high purity (99.95%) pre-mixed H<sub>2</sub>-He (Matheson Gas) into 350-400  $\mu\text{m}$  beryllium copper (BeCu) gaskets. The hydrogen-helium mixtures were loaded by pressuring the gas mixtures to supercriticality inside the sample chamber before clamping the cell. 5 $\mu\text{m}$  rubies were used as a pressure calibration<sup>40,41</sup>. The direct measurement of the ruby in a low-density fluid media may have the ruby's luminescence heat the sample, which may overestimate the pressure<sup>42</sup>. To ensure the reference ruby wavelength is measured from ambient temperature, the R<sub>1</sub> ruby line was measured at atmospheric pressure (0.1 MPa) with decreasing power down to < 1 mW and then extrapolated to 0 mW. Cells were then pressurized to 0.5-1 GPa to seal the mixture inside the cell before measurements.

The Brillouin scattering measurements were performed at GSECARS (Sector 13) at the Advanced Photon Source. The instrument is an on-line Brillouin system that allows for simultaneous X-ray and Brillouin measurements<sup>43</sup>. X-ray measurements were performed on the gasket material to identify possible hydrogen diffusion into the gasket and subsequent hydride formation. We used a scattering angle of  $\theta_i = 50$  degrees and an excitation laser wavelength of  $\lambda_l = 532\text{nm}$ .

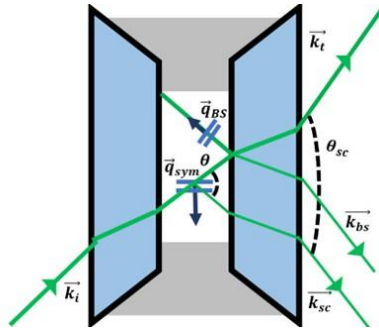


**FIG. 2.** A sidereal view of a sample inside the gasket of a DAC in a symmetric scattering geometry.

Brillouin scattering measures the transfer momentum  $\vec{k}_{SC} = \vec{k}_l \pm \vec{q}$  and provides the inelastic scattering frequency shift,  $\Delta\nu = \vec{q}$ . The Brillouin shift,  $\Delta\nu$ , may be expressed in terms of acoustic velocity  $U$ , excitation laser wavelength  $\lambda_l$ , and  $\theta$ , the angle between the incident and scattered wavevectors.

$$\Delta\nu = 2U_l k \sin\left(\frac{\theta}{2}\right) = \frac{2U_l}{\lambda_l} n_{\text{H}_2:\text{He}} \sin\left(\frac{\theta}{2}\right) \quad (4)$$

All cells were measured using a symmetric scattering geometry, which is independent of the index of refraction  $n$ . Using Sell's law and  $n_{\text{air}} \cong 1$ ,  $n_{\text{H}_2:\text{He}} \sin\left(\frac{\theta}{2}\right) = \sin\left(\frac{\theta_{sc}}{2}\right)$ . The sound velocity is a function of the scattering angle  $\theta_{sc}$ , the incident laser wavelength  $\lambda_l$ , and the Brillouin shift.

$$U_{l,sym} = \frac{\lambda \Delta\nu}{2 \sin\left(\frac{\theta_{sc}}{2}\right)} \quad (5)$$

The backscattering peaks represented by  $\theta_i = 180^\circ$ , can be used to directly calculate an index of refraction:

$$n = \frac{U_{l,sym}}{\sin\left(\frac{\theta_{sc}}{2}\right) U_{l,bs}} \quad (6)$$

The back-scattering measurements were limited to lower pressures due to limitations of the range of frequencies measured by the Brillouin system.

### III. Results

Brillouin spectra for 1:1 and 9:1 mixtures were measured from 0.5 to 5.4 GPa between 294-298 K. The frequency shifts were converted into sound velocity with Eq. (5).

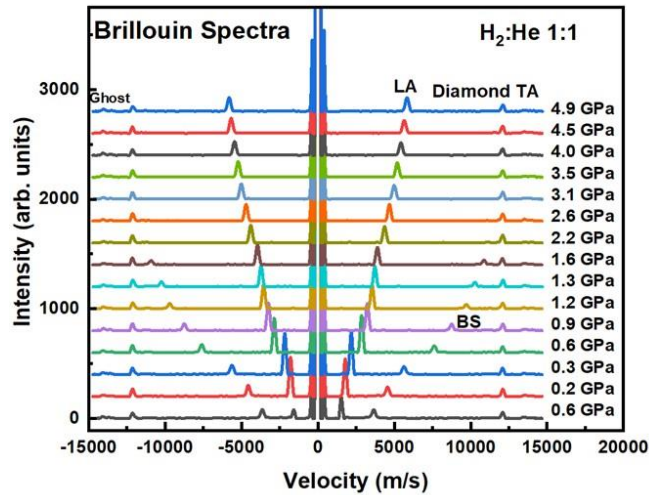


**FIG. 3.** Representative Brillouin spectra converted to sound velocities. The symmetric longitudinal acoustic (LA) and back-scattered (BS) peaks from the 1:1 H<sub>2</sub>:He sample, and the transverse acoustic (TA) mode of the diamond are measured within the frequency range available to the spectrometer. The ghost peak is a result of the Brillouin spectrometer's limit of the free spectral range, limiting higher frequency measurements.<sup>44</sup>

In order to compare the 1:1 and 9:1 mixtures to an ideal mixing model, reference curves were established using data in Fig. 1. These were fit to a modified power law equation of state  $U_l = AP^B e^{-CP}$ , which will be discussed in a later section. This region matches well with a liquid-like H<sub>2</sub> and He. The 1:1 and 9:1 ideal reference curves were calculated using the adiabatic ideal sound velocity mixing equation<sup>45</sup>.

$$U_{H_2:He} = \frac{x_{H_2} \sqrt{M_{H_2}} U_{H_2} + x_{He} \sqrt{M_{He}} U_{He}}{x_{H_2} \sqrt{M_{H_2}} + x_{He} \sqrt{M_{He}}} \quad (7)$$

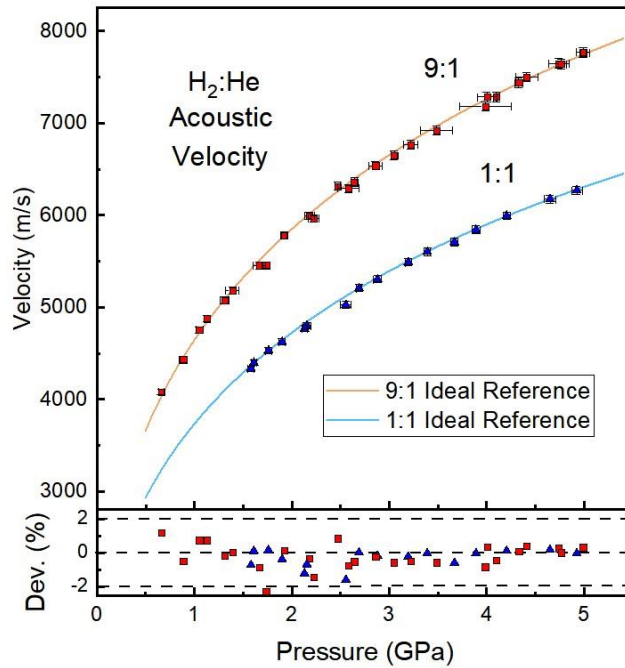


**FIG. 4.** Velocity measurements compared to a reference ideal mixing curves for 1:1 and 9:1 mixture. Residuals of the ideal mixing curve with the measured velocity data. There is very little deviation over the range measured with no indication of a trend of increasing or decreasing deviation, with an average deviation of -0.4% and 0.3% for 9:1 and 1:1, respectively.

Our measured velocity indicates very close agreement with the ideal mixing references used, with our data deviating less than 1% over the pressure range measured. This indicates very little interaction from 0.5 GPa through H<sub>2</sub> freezing pressure at 5.4 GPa. This allows us to assume low interactions between the H<sub>2</sub> and He specimens. We use this observation to assume the ideality of

the  $\gamma$ -factor in Eq. (3) as well as assume the ideal mixing of the H<sub>2</sub>:He mixtures above the 1 GPa 300 K mixing studied by Ree *et. al.*<sup>36</sup>. This assumption may break down above 1 GPa. The initial pressure of the 1:1 H<sub>2</sub>:He EOS is 1.58 GPa, which may introduce an error in this assumption. Duwal *et al.* indicate approximately up to a 2% non-ideality at higher pressures<sup>15</sup>.

Density was calculated with a trapezoidal integration scheme on Eq. (3)

$$\rho - \rho_0 = \int_{P_0}^P dP \frac{\gamma}{U_l^2} \cong \sum_{i=1}^N \frac{1}{2} \left[ \frac{\gamma(P_i)}{U_l(P_i)^2} + \frac{\gamma(P_{i+1})}{U_l(P_{i+1})^2} \right] \Delta P \quad (8)$$

Due to low interaction between the species at 1:1 and 9:1 ratio, the  $\gamma$ -factor and initial density  $\rho_0$  were assumed to mix ideally to 1.5 GPa. The mixed gamma factors were calculated by fitting previous gamma factor measurements for the H<sub>2</sub><sup>22, 46</sup> and He<sup>20, 30, 47</sup> end members. The initial density at 1:1 and 9:1 was calculated with linear mixing of the EOS determined by Mills *et al.*<sup>34</sup> for He and Matsuishi *et al.*<sup>22</sup> for H<sub>2</sub>.

The power-law<sup>24, 32</sup> and Benedict EOS.<sup>22</sup> were employed to represent the densities as a function of pressure. The number of variables used in the Benedict EOS was varied to determine the best fit with the least mutual dependency on the coefficients. A least-squares regression algorithm was used to determine the parameters and their respective errors; this process has been outlined in detail for the H<sub>2</sub> system<sup>22</sup>.

A power-law EOS,

$$\rho_{PL} = AP^B \quad (9)$$

is valid over a range of pressures for fluid H<sub>2</sub> and He but fails as the low-pressure gas. The Benedict EOS,

$$\rho_{Bene} = \frac{M_{H_2:He}}{AP^{-\frac{1}{3}} + BP^{-\frac{2}{3}} + CP^{-1}} \quad (10)$$

compensates for this failure with higher-order terms to allow for lower-pressure corrections.

The ideal mixing reference curves were calculated by integrating the ideal mixing velocity Eq. (7) with Eq. (8). The ideal reference densities were fitted to Eq. (10). We therefore define the non-ideality  $Y$  as

$$Y = \frac{1}{\rho_{id}(P)} \left( \int_{P_0}^P dP \frac{\gamma}{U_l^2} - (\rho_{id}(P) - \rho_{id}(P_0)) \right) + \frac{\delta\rho(P_0)}{\rho_{id}(P)} \quad (11)$$

which includes both the non-ideality of the density as a function of pressure and of the reference density  $\rho(P_0)$ .

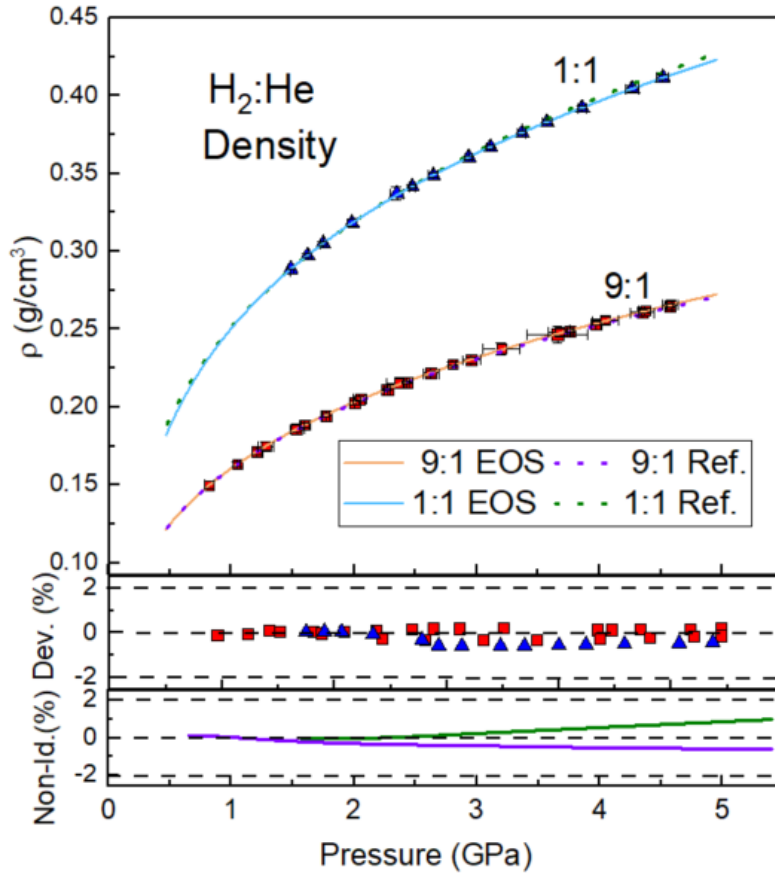


**FIG. 5.** A comparison of the measured densities, the 3-parameter Benedict EOS, and reference densities. Residuals and non-ideality are also compared.

The power law and Benedict EOS accurately represent the calculated density over the pressure range. To determine the relative deficiencies, if any, for the Benedict EOS, we set the C and B parameters equal to zero respectively; an issue with a higher number of free-fitting parameters is the increased uncertainty of the values of the fitted coefficients. We report the value of the coefficients, the Pearson's  $r^2$  goodness-of-fit value. Errors in parameters are provided to show uncertainties generated by mutual dependencies and uncertainty from the fits.

**Table 1.** Comparison of 1:1 and 9:1 EOS, their uncertainties, goodness of fit, and standard deviation of the calculated density with the equations of state.

9:1 H <sub>2</sub> :He	Power Law $\rho = AP^B$	Benedict $A, B, C \neq 0$	Benedict $A, B \neq 0$
		2.22 $AP^{-\frac{1}{3}} + BP^{-\frac{2}{3}} + CP^{-1}$	2.22 $AP^{-\frac{1}{3}} + BP^{-\frac{2}{3}}$
A	0.1572( $\pm 0.002$ )	15.5( $\pm 0.3$ )	14.46( $\pm 0.05$ )
B	0.327( $\pm 0.001$ )	-3.3( $\pm 0.6$ )	-0.34( $\pm 0.07$ )
C	0	1.9( $\pm 0.4$ )	0
Pearson R <sup>2*</sup>	0.9997	0.9998	0.9997
$\sigma_\rho$ (%)*	0.198	0.230	0.229

1:1 H <sub>2</sub> :He	Power Law $\rho = AP^B$	Benedict $A, B, C \neq 0$	Benedict $A, B \neq 0$
		3.01 $AP^{-\frac{1}{3}} + BP^{-\frac{2}{3}} + CP^{-1}$	3.01 $AP^{-\frac{1}{3}} + BP^{-\frac{2}{3}}$
A	0.2495( $\pm 0.005$ )	15.2( $\pm 0.3$ )	12.95( $\pm 0.07$ )
B	0.315( $\pm 0.007$ )	-7.4( $\pm 0.6$ )	-0.9( $\pm 0.1$ )
C	0	4.6( $\pm 0.6$ )	0
Pearson R <sup>2*</sup>	0.9996	0.9999	0.99891
$\sigma_\rho$ (%)*	0.174	0.277	0.276

\*The high-accuracy EOS requires both an  $r^2$  near unity and little variability of the data compared to the EOS model. The standard deviations for both pressure and density for all fitting equations are less than 0.3%.

With the two-parameter Benedict EOS, the deviation of the measured data from the fit is within 0.3%. The trends do indicate that there is an increased deviation of the density by pressure, however, it is still well-constrained over the whole range of interest here. The non-ideality of velocity does not quite carry over to the density: the assumptions of ideal mixing of the  $\gamma$  factor and the initial density seem well-founded, however, the greater non-ideality at higher pressures for the 1:1 mixture is above mathematical and experimental uncertainty.

The index of refraction was calculated using Eq. (6). This method has limitations due to the resolution of the Brillouin symmetric and backscattering peaks, however, it still is useful in developing a picture of its behavior. The calculated index of refraction measurements was compared against the ideal mixing scenario.

Using the fact that hydrogen and helium indicate ideal mixing, a well-known equation relating the index of refraction to the polarizability and its density, the Lorentz-Lorenz relationship, may be used<sup>48</sup>.

$$\frac{n^2 - 1}{n^2 + 2} = \frac{4\pi}{3} N_A \alpha \quad (12)$$

where  $N_A$  is Avogadro's number and  $\alpha$  is the polarizability. This may be rearranged in terms of density as

$$\frac{1}{\rho} \frac{(n^2 - 1)}{n^2 + 2} = \frac{4\pi}{3} \left( \frac{V}{M} \right) N_A \alpha \quad (13)$$

Assuming ideal mixing, the term  $\frac{V}{M} N_A$  may be broken up into weight-fractions of the hydrogen and helium components of the mixture,  $w_{H_2}$ ,  $w_{He}$

$$\frac{1}{\rho} \frac{(n_{H_2:He}^2 - 1)}{n_{H_2:He}^2 + 2} = w_{H_2} \left( \frac{4\pi}{3} N_A \alpha_{H_2} \right) + w_{He} \left( \frac{4\pi}{3} N_A \alpha_{He} \right) \quad (14)$$

Reapplying the Lorenz-Lorentz relationship to the  $H_2:He$  system

$$\frac{1}{\rho} \frac{(n_{H_2:He}^2 - 1)}{(n_{H_2:He}^2 + 2)} = w_{H_2} \left( \frac{1}{\rho} \frac{(n_{H_2}^2 - 1)}{(n_{H_2}^2 + 2)} \right) + w_{He} \left( \frac{1}{\rho} \frac{(n_{He}^2 - 1)}{(n_{He}^2 + 2)} \right) \quad (15)$$

The indices of refraction  $n_{H_2}$ ,  $n_{He}$  were from Dewaele *et. al*<sup>27</sup> and the densities  $\rho_{H_2}$ ,  $\rho_{He}$ ,  $\rho_{H_2:He}$  were taken from the EOS determined here.

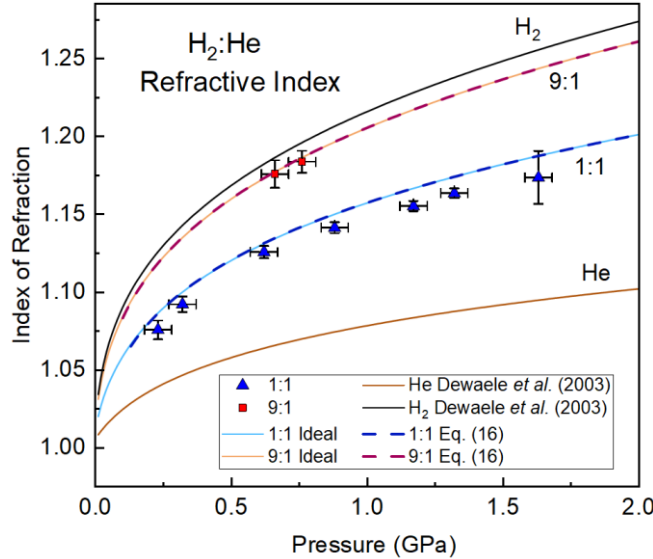


**FIG. 6.** Pressure dependence of the index of refraction calculated by Eq. (6)<sup>27</sup> and that used in Ref. <sup>15</sup>. The orange and blue lines show ideal mixing result.

The measured index of refraction differs from the prediction of ideal mixing by <2% for 9:1  $H_2:He$ , whereas the measured values for 1:1  $H_2:He$  are significant lower than the ideal mixing curve. The discrepancy may be due to loss of  $H_2$  to the stainless-steel gaskets that were used. We suggest that ideal mixing may be assumed for these in future dynamic compression experiments using a power law of the form

$$n(P) = a + b(1 + P)^c \quad (16)$$

**Table 2.** Coefficients for power-law relation for pressure dependence of the index of refraction assuming ideal mixing.

Composition	a	b	c
9:1	0.951±0.001	0.255±0.001	0.284±0.001
1:1	0.927±0.003	0.231±0.003	0.250±0.003

## IV. Discussion

### A. Equations of State

Several high-pressure fluid equations of state have been successfully applied to the H<sub>2</sub> and He up to several gigapascals, specifically the power law (H<sub>2</sub><sup>21,24</sup>) and Benedict (H<sub>2</sub><sup>22,26,33</sup> and He<sup>34</sup>) EOS. The power law EOS has been used to describe the relationship between the sound velocity and pressure for liquids and modestly compressed fluids<sup>49,50</sup> and is based on the observation that  $\frac{d \ln(U_l)}{d \ln(P)}$  is close to constant over a range of pressures. Integration leads to Rao's law<sup>50</sup>

$$U = AP^B, \quad (17)$$

where  $A$  reflects an initial condition and  $B$  is the constant of proportionality, which has been to be about 1/3.<sup>24,50</sup> Due to the broad application to many different liquids and liquid-like fluids, this EOS represents H<sub>2</sub> and He supercritical fluids at higher pressures.

The Benedict-type EOS<sup>51</sup> is a  $P$ - $V$ - $T$  EOS that has been used for compressible fluids over a wide range of pressures and temperatures,

$$V(P, T) = \sum_{j=1}^3 \sum_{l=-2}^2 A_{l,j} P^{-\frac{j}{3}} T^{\frac{l}{2}} \quad (18)$$

The usefulness of the Benedict EOS arises from it containing the two independent variable system with highly tunable coefficients to allow for a range of  $P$ - $T$  conditions.<sup>34</sup> We focus on the room temperature (296 K) isotherm in this study; however, this EOS has been used extensively for H<sub>2</sub> up to 5.4 GPa 600 K<sup>22</sup>. Fewer studies have applied the Benedict-type equation of state on helium, at the relevant pressures and temperatures to this study.<sup>28,34</sup> The applicability of the Benedict EOS can be assessed from its limiting cases. At high pressure, we expect Eq. (18) to have  $A_2 P^{-\frac{2}{3}}$  and  $A_3 P^{-1}$  become negligible compared to  $A_1 P^{-\frac{1}{3}}$ . This reflects the power-law EOS, which  $\rho_{PL}, U_{PL,l} \sim P^{-\frac{1}{3}}, P^{\frac{1}{3}}$ . At low pressures, the  $A_3 P^{-1}$  term dominates, which reproduces the ideal gas law, highlighting the origin of the low pressure deviations seen in the power-law equation of state in Fig. 7.

## B. Reference EOS

Three equations of state were employed to fit sound velocity data for  $\text{H}_2$ <sup>21-23, 26, 33</sup> and  $\text{He}$ <sup>28, 30, 34</sup> to establish a reference density using Eq. (3) at our reference temperature of 296 K. Low dependence of temperature on density enables us to use several different studies on  $\text{H}_2$  and  $\text{He}$  to establish end member velocity equation. A Benedict-type,  $U = \sum_{i=1}^3 A_i P^{\frac{i}{3}}$ , power law,  $U = AP^B$ , and a modified exponential power law,  $U = AP^B e^{CP}$  EOS were fit to the velocity data to determine the best fit. Each equation was analyzed for the overall deviation of the experimental values from our reference curve.

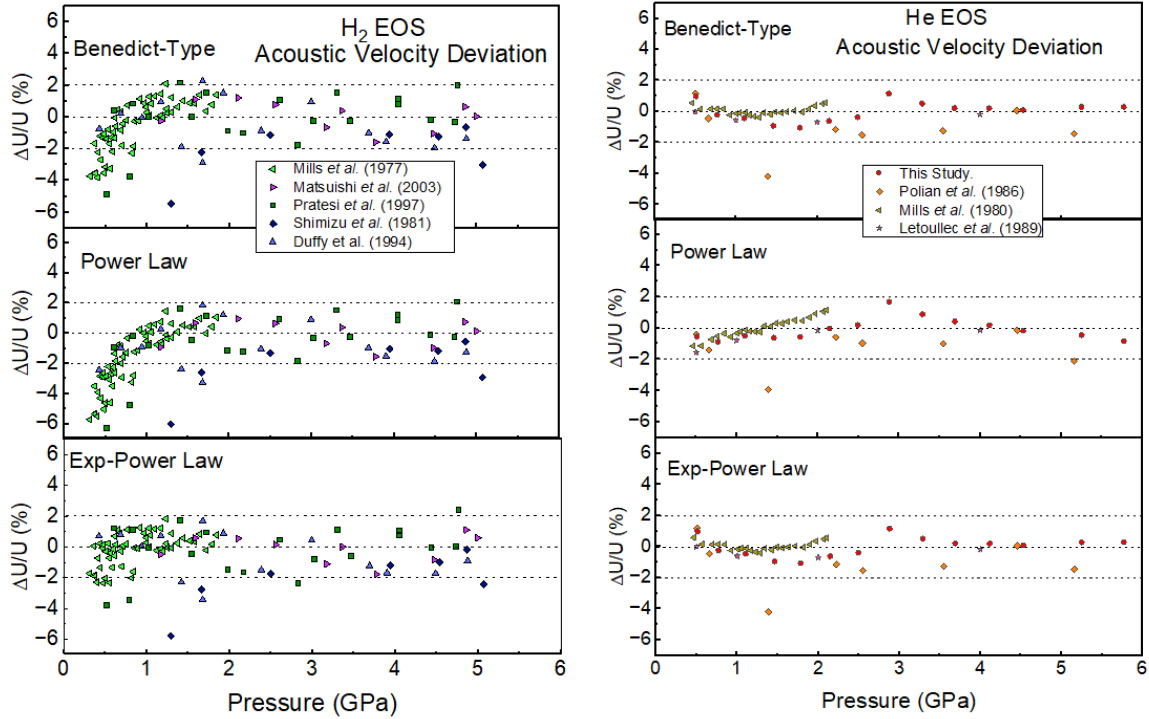


**FIG. 7.** Comparison of the  $U$ - $P$  relations determined here with previous results for  $\text{H}_2$ <sup>21-24, 33</sup> and  $\text{He}$ <sup>28, 30, 34</sup>

The modified power-law EOS had the lowest deviation for both  $\text{H}_2$  and  $\text{He}$  (0.47% and 0.35% respectively), then the Benedict-type velocity EOS (0.58% and 0.36% respectively), followed by the power law model (0.52% and 0.70% respectively). The power-law EOS deviated the most from the data in the lower pressure region, which still preserves non-liquid-like behavior. This deviation is accounted for in the higher-order terms in the Benedict-type and the modified power law equations.

The densities of the  $\text{H}_2$  and  $\text{He}$  were calculated with the determined reference acoustic velocities using Eq. (3). These are compared against previous  $\rho$ - $P$  EOS for  $\text{H}_2$ <sup>22, 23, 26, 32, 33</sup> and  $\text{He}$ <sup>28, 30, 34</sup>

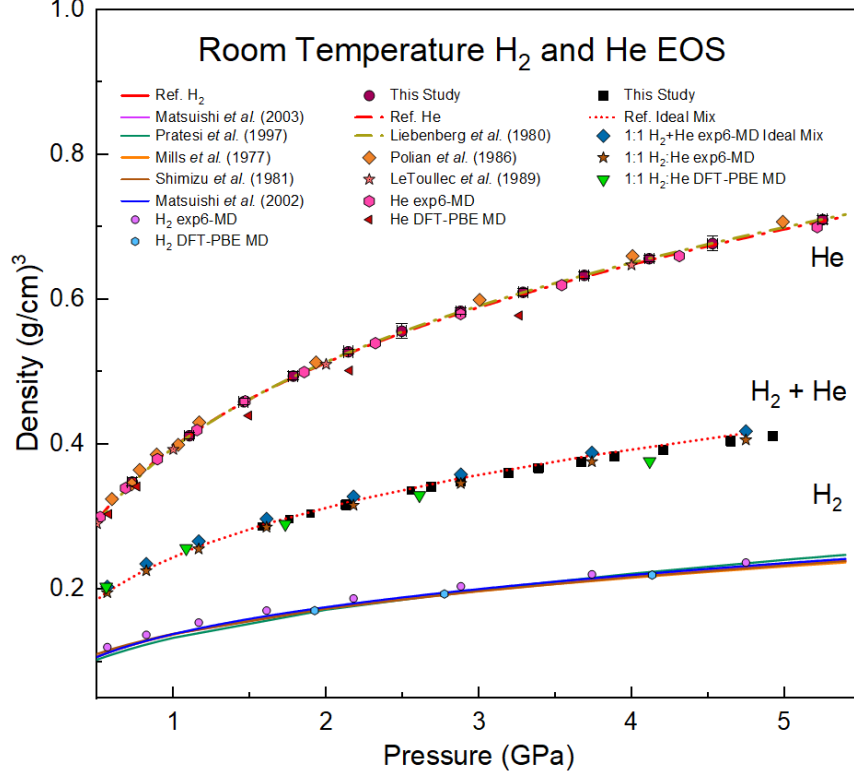


**FIG. 8.** Comparison of  $H_2$  and He  $\rho$ - $P$  at room temperature (293 K - 300 K) from 0.5 to 5.4 GPa. These densities were determined experimentally in this and previous<sup>21, 22, 33</sup> studies, as well as an MD simulation without a nuclear quantum effects (NQE) corrections.<sup>15</sup> The solid lines correspond to the EOS from Refs.<sup>21, 22, 24, 26, 33, 34</sup>

The hydrogen reference density used here and by Matsuishi *et al.*<sup>22</sup> work very well over the whole range analyzed, with a deviation at the highest pressures of 0.8%. The  $\rho$ - $P$  EOS of Pratesi *et al.*<sup>21</sup> and Shimizu *et al.*<sup>32</sup> overestimate the density at lower pressures but show better agreement with the present work at higher pressures; notably, a power-law was used to represent the EOS in these studies.<sup>21 32</sup> The Mills *et al.*<sup>33</sup> EOS agrees well with Matsuishi *et al.*<sup>26</sup> and that obtained here over the 0.2 to 2.0 GPa pressure range, with a  $\sim 1.5\%$  density deviation between the studies at  $H_2$  freezing. Mills *et al.*<sup>34</sup> used a Benedict EOS to accurately model He from 0.2 to 2.0 GPa. All  $\rho$ - $P$  results for He are in good agreement ( $\delta\rho < 0.5\%$ ) with the exception of the data of Polian *et al.*<sup>30</sup>; ( $\delta\rho \sim 1.5\%$ ); this discrepancy is due to the approximate  $\gamma$  factor used in this early study.<sup>28</sup>

We now compare the experimental results with various simulations. Ree<sup>36</sup> examined the EOS and other properties fluid  $H_2$ , He, and  $H_2$ -He mixtures up to 1 GPa using an exp-6 potentials for all interactions, i.e.,

$$\phi_{E6}(r) = \frac{\epsilon}{\alpha - 6} \left[ e^{\alpha \left(1 - \frac{r}{r^*}\right)} - \alpha \left(\frac{r^*}{r}\right)^6 \right], \quad (19)$$

The  $H_2$ -He interaction used  $\epsilon/k_b = 36.4\text{K}$ ,  $r^* = 3.43\text{\AA}$ ,  $\alpha = 11.1$ . For He-He, we used  $\epsilon/k_b = 10.57\text{K}$ ,  $r^* = 2.97\text{\AA}$ ,  $\alpha = 13.6$ . Finally for  $H_2$ -He, we used  $\epsilon/k_b = 15.5\text{K}$ ,  $r^* = 3.37\text{\AA}$ ,  $\alpha = 12.7$ .<sup>15,36</sup>

This parameterization of the exp-6 potential starts to exhibit noticeable departures from the experimentally determined of H<sub>2</sub> and He isotherms around the highest pressure ranges of the present study. To establish a rough order of magnitude for the size of the nuclear quantum corrections in H<sub>2</sub> and H<sub>2</sub>+He, we performed path integral molecular dynamics simulations using the aforementioned classical potentials at densities of 0.035, 0.075, and 0.0145 mol/cc, which corresponds to the pressure range 0.1-3GPa. This data was used to interpolate nuclear quantum corrections to the energy and pressure within the same pressure range for our isotherm. We find that the effect on the 300K isotherm is roughly a 3% reduction in the density, thus accounting for a large part of the discrepancy. Such details are of course extremely important to construct an accurate equation of state, but for future discussions of non-ideality of mix, we will ignore nuclear quantum effects for simplicity. In any case, below 3GPa, the classical molecular dynamics does a very good job matching the experimentally measured equations of state and will serve as a reasonable model for assessing nonideal mixing effects.

To complement the classical potential molecular dynamics simulations, we also ran some density functional theory molecular dynamics calculations using the PBE functional. We find that hydrogen is in very good agreement with previous experimental data, whereas helium is systematically softer than experiment across all considered densities. This amounts to a roughly 4% higher density than experiment over all pressures. Some of this could be due to the choice of functional—PBE was chosen for its transferability to more extreme pressure and temperature regimes, rather than as an *a posteriori* choice to match our experimental data. Most likely, however, the same neglect of nuclear quantum effects observed in the classical potential equations of state are carrying over to the DFT calculations.

### C. Ideality of Mixing

We now examine more quantitatively the non-ideality of mixing on various properties obtained from the experiment and simulations for the H<sub>2</sub>:He system. Non-ideality is defined as the excess density of mixing as seen in Eq. (11), where the term  $\frac{\delta\rho}{\rho_{1d}}$  represents the excess initial density term. This study’s assumption of ideally mixed reference densities was compared against computational results also found in Ref.<sup>15</sup> The exponential-6 potential seen in Eq. (19) was used for classical potential molecular dynamics simulations (exp-6-MD) of the H<sub>2</sub>-He system. These exp6-MD simulations indicate approximately a 4% non-ideality and 1% at the starting pressures for 1:1 and 9:1 H<sub>2</sub>:He respectively.

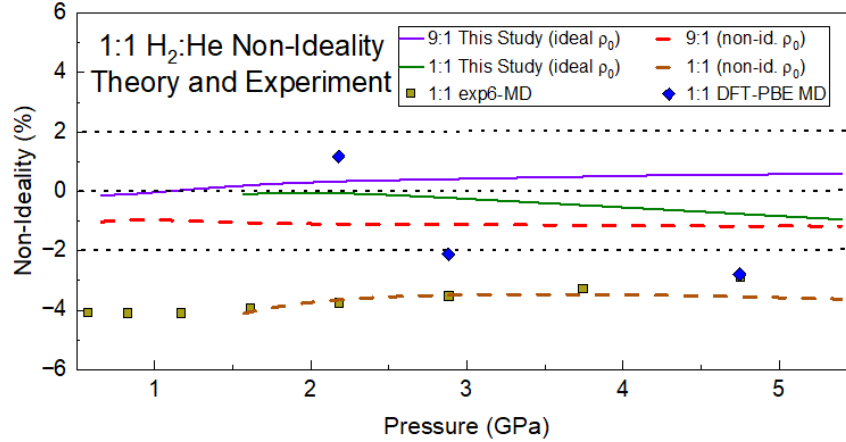


**FIG. 9.** Comparison of the experimentally and computationally determined non-ideality using Eq. (11). Reported computational EOS used DFT-PBE (blue diamonds) and exponential-6 Eq. (19) classical potential molecular dynamic simulations (gold squares) are compared against this study’s 1:1 and 9:1 non-ideality calculated through Eq. (11). details of the simulations are provided in Ref.<sup>15</sup> Also plotted are the non-idealities for 1:1 and 9:1 mixtures calculated using a non-zero  $\delta\rho/\rho_{id}$  obtained through exp6-MD simulations (red and gold dashed lines).

Overall, the classical potential simulations<sup>15, 36</sup> agree well with the experimental results for 1:1 H<sub>2</sub>:He values. On the other hand, the H<sub>2</sub>:He DFT-PBE MD calculation (Fig. 8) agrees well at higher pressures, however the non-ideality raises substantially at lower pressures; below 2.0 GPa, the non-ideality is larger than the range of Fig. 9. The jump in non-ideality below 2.5GPa can be attributed to several things—lack of dispersion interactions in the PBE functional which become more important (in a relative sense) as the density is decreased, or poor sampling at lower pressures that might bias the fit, but neither of these facts are especially surprising.

As an estimation of the importance of the  $\delta\rho/\rho_{id}$  term in Eq. (11), the non-ideality of the 1:1 and 9:1 H<sub>2</sub>:He exp6-MD simulations were used. The 1:1 H<sub>2</sub>:He non-ideality indicates a non-ideality of approximately 3-4% while the 9:1 H<sub>2</sub>:He exp6-MD simulation indicates a smaller non-ideality of approximately 1%. This observation should be taken with caution. The contribution of non-ideality from the deviation in density is comparatively small relative to the non-idealities due to non-ideal initial density based on the exp6-MD simulations. The H<sub>2</sub> and He systems are notoriously difficult to model<sup>1</sup> and this study is looking at a difference of a few percent. Careful volumetric measurements will need to be taken on H<sub>2</sub>:He mixtures to resolve small non-ideal effects in the initial pressure range of this experiment.

#### D. Gasket Effects

Finally, we consider the possibility of changing the bulk composition of the mixture by diffusion or reaction of the fluid samples with the gasket. The Brillouin scattering shift as well as the Q<sub>1</sub>(1) H<sub>2</sub> vibron are both highly dependent on the relative concentration of H<sub>2</sub> in the system.<sup>37, 38, 52-54</sup> The strong dependence of the Q<sub>1</sub>(1) vibron on helium composition can be used as a gauge of the concentration of the hydrogen relative to the initial composition. Higher concentrations of helium decrease the interaction of hydrogen molecules with respect to one another, causing a blueshift in the Q<sub>1</sub>(1) vibron. This effect is notable: a pure H<sub>2</sub> mixture has an ambient vibron frequency of 4150 cm<sup>-1</sup> at 0.1 MPa, increasing to 4200 cm<sup>-1</sup> at 5.4 GPa at 300 K, whereas the vibron of an isolated H<sub>2</sub> molecule in fluid He can shift up to 4300 cm<sup>-1</sup> at 5.4 GPa at 300 K.<sup>52, 54</sup>

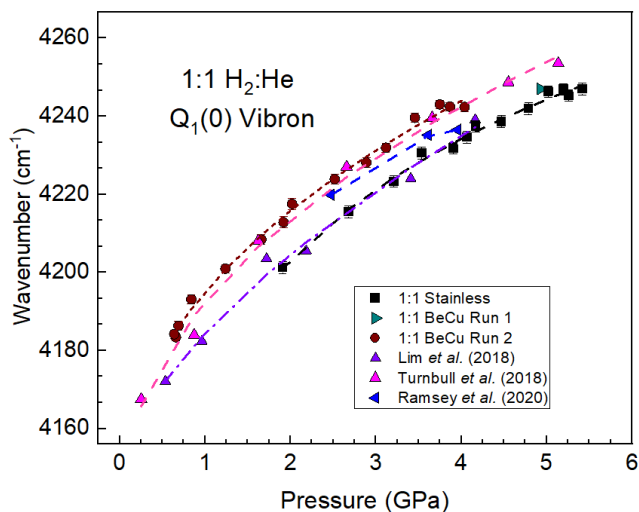


**FIG. 10.** Pressure dependence of the  $Q_1$  vibron Raman frequency for  $H_2:He$  mixtures measured at room temperature using different gasket materials in DACs. The previous results are from Refs. <sup>37, 54, 55</sup>. Dashed lines are guides to the eye.

The acoustic sound velocity is highly dependent on the relative concentration of He in the mixture. The more helium, the slower the mixture will be. Comparing the data measured in the BeCu gaskets and the stainless-steel gaskets, BeCu gaskets indicate a more accurate fit relative to the ideal mixing case compared to stainless steel. On the other hand, stainless-steel gaskets show an overall decrease in the velocity relative to ideal mixing. This is likely due to  $H_2$  diffusing much more rapidly into stainless steel compared to BeCu. Due to variable times between loading and measuring (1-3 days), the BeCu shows less deviation over the whole pressure range measured. The observed decrease in the sound velocities of all stainless-steel runs after approximately 3.0-3.5 GPa is attributed to reaction of hydrogen with gasket to form iron hydride,<sup>56</sup> which is known to occur in DAC experiments.<sup>32</sup> Similar effects would occur with the use of other metals as gaskets such as Re<sup>57</sup> and W.<sup>58</sup>

□

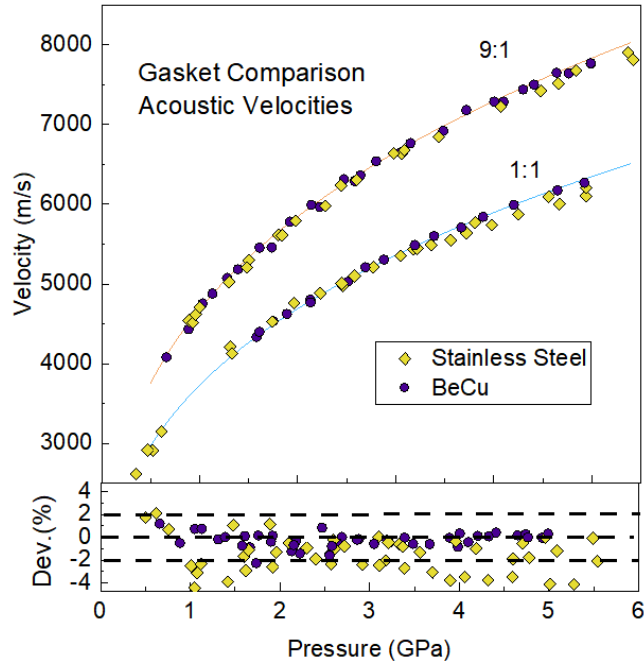


**FIG. 11.** Sound velocities of mixtures measured using stainless steel and BeCu gaskets, together with the deviation from that determined for the BeCu experiments assuming ideal mixing.

## V. Conclusions

Two  $\rho$ - $P$  EOS have been developed for  $H_2:He$  mixtures to within 0.3% accuracy in density up to 5 GPa at room temperature through the use of Brillouin scattering. Sound velocity measurements indicate ideal mixing for 1:1 and 9:1  $H_2:He$  samples analyzed within an average of -0.4% for 9:1 and 0.3% for 1:1. The  $\rho$ - $P$  EOS of the mixtures are close to that expected for ideal mixing, but there is evidence of systematic non-ideality reaching 1.1% for 1:1  $H_2:He$ . The results are consistent with early simulations using classical effective potentials. The comparison of the experimental results with DFT calculations provides tests of both the use of such techniques for low-pressure mixtures of these fundamental elements as well as of assumption made in obtaining the EOS from the Brillouin measurements. The EOS developed provides a set of initial conditions for dynamic compression experiments using precompressed  $H_2:He$  mixtures. Further studies include the effect of temperature to determine full  $P$ - $\rho$ - $T$ - $X$  EOS, including higher pressures possible using these static compression techniques.

## Acknowledgments

This work was supported by the Department of Energy (DOE) and the National Nuclear Security Administration (NNSA) through the Chicago/DOE Alliance Center (DE-NA003975). Portions of this work were performed at GeoSoilEnviroCARS (Sector 13), Advanced Photon Source (APS), and Argonne National Laboratory (ANL). GeoSoilEnviroCARS is supported by the National Science Foundation (EAR-1634415). This research used resources of the APS, a U.S. DOE Office of Science User Facility operated for the DOE Office of Science by ANL under Contract No. DE-AC02-06CH11357. Sandia National Laboratories is a multimission laboratory managed and operated by National Technology and Engineering Solutions of Sandia, LLC, a wholly-

owned subsidiary of Honeywell International Inc., for the DOE-NNSA (DE-NA0003525). This paper describes objective technical results and analysis. Any subjective views or opinions that might be expressed in this paper do not necessarily represent the views of the U.S. Department of Energy of the United States Government.

1. J. M. McMahon, M. A. Morales, C. Pierleoni and D. M. Ceperley, "The properties of hydrogen and helium under extreme conditions," *Rev Mod Phys* **84**, 1607-1653 (2012).
2. D. J. Stevenson, "Jupiter's interior as revealed by Juno," *Annu. Rev. Earth Planet* **48**, 465-489 (2020).
3. T. Sano, N. Ozaki, T. Sakaiya, K. Shigemori, M. Ikoma, T. Kimura, K. Miyanishi, T. Endo, A. Shiroshita and H. Takahashi, "Laser-shock compression and Hugoniot measurements of liquid hydrogen to 55 GPa," *Phys. Rev. B* **83**, 054117 (2011).
4. P. Loubeyre, P. M. Celliers, D. G. Hicks, E. Henry, A. Dewaele, J. Pasley, J. Eggert, M. Koenig, F. Occelli, K. M. Lee, R. Jeanloz, D. Neely, A. Benuzzi-Mounaix, D. Bradley, M. Bastea, S. Moon and G. W. Collins, "Coupling static and dynamic compressions: first measurements in dense hydrogen," *High Pressure Research* **24**, 25-31 (2004).
5. P. Loubeyre, S. Brygoo, J. Eggert, P. M. Celliers, D. K. Spaulding, J. R. Rygg, T. R. Boehly, G. W. Collins and R. Jeanloz, "Extended data set for the equation of state of warm dense hydrogen isotopes," *Phys. Rev. B* **86**, 144115 (2012).
6. M. D. Knudson, M. P. Desjarlais, A. Becker, R. W. Lemke, K. R. Cochrane, M. E. Savage, D. E. Bliss, T. R. Mattsson and R. Redmer, "Direct observation of an abrupt insulator-to-metal transition in dense liquid deuterium," *Science* **348**, 1455-1460 (2015).
7. M. D. Knudson, D. L. Hanson, J. E. Bailey, R. W. Lemke, C. A. Hall, C. Deeney and J. R. Asay, "Equation of state measurements in liquid deuterium to 100 GPa," *J. Phys. A* **36**, 6149 (2003).
8. P. M. Celliers, M. Millot, S. Brygoo, R. S. McWilliams, D. E. Fratanduono, J. R. Rygg, A. F. Goncharov, P. Loubeyre, J. H. Eggert, J. L. Peterson, N. B. Meezan, S. L. Pape, G. W. Collins, R. Jeanloz and R. J. Hemley, "Insulator-metal transition in dense fluid deuterium," *Science* **361**, 677-681 (2018).
9. C. T. Seagle, W. D. Reinhart, A. J. Lopez, R. J. Hickman and T. F. Thornhill, "High precision Hugoniot measurements on statically pre-compressed fluid helium," *J. Appl. Phys.* **120** (2016).
10. J. H. Eggert, P. M. Celliers, D. G. Hicks, J. R. Rygg, G. W. Collins, S. Brygoo, P. Loubeyre, R. S. McWilliams, D. Spaulding and R. Jeanloz, presented at the AIP, 2009 (unpublished).
11. M. Preising, W. Lorenzen, A. Becker, R. Redmer, M. D. Knudson and M. P. Desjarlais, "Equation of state and optical properties of warm dense helium," *Phys. Plasmas* **25** (2018).
12. P. M. Celliers, P. Loubeyre, J. H. Eggert, S. Brygoo, R. S. McWilliams, D. G. Hicks, T. R. Boehly, R. Jeanloz and G. W. Collins, "Insulator-to-conducting transition in dense fluid helium," *Phys. Rev. Lett.* **104**, 184503 (2010).
13. P. M. Kowalski, S. Mazevet, D. Saumon and M. Challacombe, "Equation of state and optical properties of warm dense helium," *Phys. Rev. B* **76**, 075112 (2007).
14. S. Brygoo, P. Loubeyre, M. Millot, J. R. Rygg, P. M. Celliers, J. H. Eggert, R. Jeanloz and G. W. Collins, "Evidence of hydrogen-helium immiscibility at Jupiter-interior conditions," *Nature* **593**, 517-521 (2021).
15. S. Duwal, R. C. C. III, M. D. Knudson, J. Boerner, K. Cochrane, J. Usher, D. Dolan, B. Farfan, C. d. L. Cruz, J. Banasek and C. T. Seagle, "Extreme compression of planetary gases: High-accuracy pressure-density measurements of hydrogen-helium mixtures above 4-fold compression," (2023).
16. S. Brygoo, M. Millot, P. Loubeyre, A. E. Lazicki, S. Hamel, T. Qi, P. M. Celliers, F. Coppari, J. H. Eggert and D. E. Fratanduono, "Analysis of laser shock experiments on precompressed samples using a quartz reference and application to warm dense hydrogen and helium," *J. Appl. Phys.* **118** (2015).
17. P. M. Celliers, M. Millot, S. Brygoo, R. S. McWilliams, D. E. Fratanduono, J. R. Rygg, A. F. Goncharov, P. Loubeyre, J. H. Eggert, J. L. Peterson, N. B. Meezan, S. Le Pape, G. W. Collins, R.

- Jeanloz and R. J. Hemley, "Insulator-metal transition in dense fluid deuterium," *Science* **361**, 677-682 (2018).
18. R. Jeanloz, P. M. Celliers, G. W. Collins, J. H. Eggert, K. M. Lee, R. S. McWilliams, S. Brygoo and P. Loubeyre, "Achieving high-density states through shock-wave loading of precompressed samples," *PNAS* **104**, 9172-9177 (2007).
  19. H. Hemmes, A. Driessen and R. Griessen, "Thermodynamic properties of hydrogen at pressures up to 1 Mbar and temperatures between 100 and 1000K," *J. Phys. C: Solid State Phys.* **19**, 14 (1986).
  20. V. D. Arp and R. D. McCarty, Report No. NIST-TN/1334, 1989.
  21. G. Pratesi, L. Ulivi, F. Barocchi, P. Loubeyre and R. LeToullec, "Hyperacoustic velocity of fluid hydrogen at high pressure," *J Phys-Condens Mat* **9**, 10059-10064 (1997).
  22. K. Matsuishi, E. Gregoryanz, H. K. Mao and R. J. Hemley, "Equation of state and intermolecular interactions in fluid hydrogen from Brillouin scattering at high pressures and temperatures," *J Chem Phys* **118**, 10683-10695 (2003).
  23. T. S. Duffly, W. L. Vos, C. S. Zha, R. J. Hemley and H. K. Mao, "Sound velocities in dense hydrogen and the interior of jupiter," *Science* **263**, 1590-1593 (1994).
  24. H. Shimizu, E. M. Brody, H. K. Mao and P. M. Bell, "Brillouin measurements of solid N-H-2 and N-D-2 to 200 kbar at room-temperature," *Phys. Rev. Lett.* **47**, 128-131 (1981).
  25. H. Shimizu, "High-pressure Brillouin scattering in a simple molecular system," *J Phys-Condens Mat* **14**, 10657-10664 (2002).
  26. K. Matsuishi, E. Gregoryanz, H. K. Mao and R. J. Hemley, "Brillouin and Raman scattering of fluid and solid hydrogen at high pressures and temperatures," *J. Phys. Condens. Matter* **14**, 10631 (2002).
  27. A. Dewaele, J. H. Eggert, P. Loubeyre and R. LeToullec, "Measurement of the refractive index and equation of state in dense He, H<sub>2</sub>, H<sub>2</sub>O, and Ne under high pressure in a diamond anvil cell," *Phys. Rev. B* **67**, 094112 (2003).
  28. R. LeToullec, P. Loubeyre and J.-P. Pinceaux, "Refractive-index measurements of dense helium up to 16 GPa at T=298K: Analysis of its thermodynamic and electronic properties," *Phys. Rev. B* **40**, 11 (1989).
  29. H. K. Mao, R. J. Hemley, Y. Wu, A. P. Jephcoat, L. W. Finger, C. S. Zha and W. A. Bassett, "High-pressure phase-diagram and equation of state of solid helium from single-crystal X-ray-diffraction to 23.3-Gpa," *Phys. Rev. Lett.* **60**, 2649-2652 (1988).
  30. A. Polian and M. Grimsditch, "Elastic properties and density of helium up to 20 GPa," *EPL* **2**, 849 (1986).
  31. Y. A. Cengel, M. A. Boles and M. Kanoğlu, *Thermodynamics: an engineering approach*. (McGraw-hill New York, 2011).
  32. E. M. Brody, H. Shimizu, H. K. Mao, P. M. Bell and W. A. Bassett, "Acoustic velocity and refractive-index of fluid hydrogen and deuterium at high-pressures," *J. Appl. Phys.* **52**, 3583-3585 (1981).
  33. R. L. Mills, D. H. Liebenberg, J. C. Bronson and L. C. Schmidt, "Equation of state of fluid n-H<sub>2</sub> from P-V-T and sound velocity measurements to 20 kbar," *J Chem Phys* **66**, 3076-3084 (1977).
  34. R. L. Mills, D. H. Liebenberg and J. C. Bronson, "Equation of state and melting properties of He 4 from measurements to 20 kbar," *Phys. Rev. B.* **21**, 5137 (1980).
  35. A. Bergermann, M. French, M. Schöttler and R. Redmer, "Gibbs-ensemble Monte Carlo simulation of H<sub>2</sub>-He mixtures," *Phys. Rev. E* **103**, 013307 (2021).
  36. F. H. Ree, "Solubility of hydrogen-helium mixtures in fluid phases to 1 GPa," *J. Phys. Chem.* **87**, 2846-2852 (1983).
  37. J. Lim and C.-S. Yoo, "Phase diagram of dense H<sub>2</sub>-He mixtures: evidence for strong chemical association, miscibility, and structural change," *Phys. Rev. Lett.* **120** (2018).
  38. P. Loubeyre, R. LeToullec and J. P. Pinceaux, "A New Determination of the Binary Phase-Diagram of H<sub>2</sub>-He Mixtures at 296-K," *J. Phys. Condens. Matter* **3**, 3183-3192 (1991).

39. W. B. Street, "Phase equilibria in molecular hydrogen-helium mixtures at high pressure," *Astrophys. J* **186**, 1107 (1973).
40. F. Datchi, A. Dewaele, P. Loubeyre, R. LeToullec, Y. L. Godec and B. Canny, "Optical pressure sensors for high-pressure-high-temperature studies in a diamond anvil cell," *High Press. Res.* **27**, 447-463 (2007).
41. G. Shen, Y. Wang, A. Dewaele, C. Wu, D. E. Fratanduono, J. H. Eggert, S. Klotz, K. F. Dziubek, P. Loubeyre and O. V. Fat'yanov, "Toward an international practical pressure scale: A proposal for an IPPS ruby gauge (IPPS-Ruby2020)," *High Press. Res.* **40**, 299-314 (2020).
42. H. K. Mao, J.-A. Xu and P. M. Bell, "Calibration of the ruby pressure gauge to 800 kbar under quasi-hydrostatic conditions," *J. Geophys. Res. Solid Earth* **91**, 4673-4676 (1986).
43. S. Sinogeikin, J. Bass, V. Prakapenka, D. Lashtenov, G. Shen, C. Sanchez-Valle and M. Rivers, "Brillouin spectrometer interfaced with synchrotron radiation for simultaneous X-ray density and acoustic velocity measurements," *Rev. Sci. Instrum.* **77**, 103905 (2006).
44. R. Mock, B. Hillebrands and R. Sandercock, "Construction and performance of a Brillouin scattering set-up using a triple-pass tandem Fabry-Perot interferometer," *J. Phys. E: Sci. Instrum.* **20**, 656 (1987).
45. H. Pfeiffer and K. Heremans, "The sound velocity in ideal liquid mixtures from thermal volume fluctuations," *ChemPhysChem* **6**, 697-705 (2005).
46. R. D. McCarty, *Selected properties of hydrogen (engineering design data)*. (US Department of Commerce, National Bureau of Standards, 1981).
47. R. D. McCarty, *Thermophysical Properties of Helium-4 from 2 to 1500 K with Pressures to 1000 Atmospheres*. (US Government Printing Office, 1972).
48. A. Z. Tasic, B. D. Djordjevic, D. K. Grozdanic and N. Radojkovic, "Use of mixing rules in predicting refractive indexes and specific refractivities for some binary liquid mixtures," *J. Chem. Eng. Data* **37**, 310-313 (1992).
49. M. R. Rao, "Velocity of sound in liquids and chemical constitution," *J Chem Phys* **9**, 682-685 (1941).
50. R. V. G. Rao and B. S. M. Rao, "Variation of sound velocity through liquids with pressure.," *Trans. Faraday. Soc.* **62**, 2704-2708 (1966).
51. M. Benedict, "Pressure, volume, temperature properties of nitrogen at high density. II. Results obtained by a piston displacement method," *J. Am. Chem. Soc.* **59**, 2233-2242 (1937).
52. P. Loubeyre, R. LeToullec and J. P. Pinceaux, "Binary phase-diagrams of H-2-He mixtures at high-temperature and high-pressure," *Phys. Rev. B* **36**, 3723-3730 (1987).
53. J. Lim, M. Kim, S. Duwal, S. Kawaguchi, S. Oishi, H.-P. Liermann, R. Hrubiak, J. S. Tse and C.-S. Yoo, "Compression behavior of dense H<sub>2</sub>-He mixtures up to 160 GPa," *Phys. Rev. B* **101**, 8 (2020).
54. S. B. Ramsey, M. Pena-Alvarez and G. J. Ackland, "Localization effects on the vibron shifts in helium-hydrogen mixtures," *Phys. Rev. B* **101**, 214306 (2020).
55. R. Turnbull, M. E. Donnelly, M. N. Wang, M. Pena-Alvarez, C. Ji, P. Dalladay-Simpson, H. K. Mao, E. Gregoryanz and R. T. Howie, "Reactivity of hydrogen-helium and hydrogen-nitrogen mixtures at high pressures," *Phys. Rev. Lett.* **121** (2018).
56. J. V. Badding, R. J. Hemley and H. K. Mao, "High-pressure chemistry of hydrogen in metals: In situ study of iron hydride," *Science* **253**, 421-424 (1991).
57. T. Atou and J. V. Badding, "In situ diffraction study of the formation of rhenium hydride at high pressure," *J. Solid State Chem.* **118**, 299-302 (1995).
58. T. A. Strobel, M. Somayazulu and R. J. Hemley, "Novel pressure-induced interactions in silane-hydrogen," *Phys. Rev. Lett.* **103**, 065701 (2009).
59. D. J. Dunstan, "Theory of the gasket in diamond anvil high-pressure cells," *Rev. Sci. Instrum.* **60**, 3789-3795 (1989).
60. C. S. Zha, T. S. Duffy, R. T. Downs, H. K. Mao and R. J. Hemley, "Sound velocity and elasticity of single-crystal forsterite to 16 GPa," *J. Geophys. Res. Solid Earth* **101**, 17535-17545 (1996).

61. S. Sinogeikin and J. Bass, "Single-crystal elasticity of pyrope and MgO to 20 GPa by Brillouin scattering in the diamond cell," *Phys. Earth Planet. Inter.* **120**, 43-62 (2000).
62. R. J. Hemley, H. K. Mao, L. W. Finger, A. P. Jephcoat, R. M. Hazen and C. S. Zha, "Equation of state of solid hydrogen and deuterium from single-crystal x-ray diffraction to 26.5 GPa," *Phys. Rev. B* **42**, 6458-6470 (1990).

## Appendix

### Error Determination and Propagation

The principal sources of error in the measurement of the pressure arises from spectrometer resolution and the drift in pressure that results from relaxation after increasing the pressure. The resolution of the spectrometer provides a smaller pressure uncertainty of 0.01 nm in the spectrometer, corresponding to a 0.03 GPa pressure error. We establish this as an uncertainty from the spectrometer's calibration. This corresponds to approximately  $\delta_{P_{inst}} = 0.03$  GPa. Pressure drift is the result of the relaxation of the DAC after an increase in pressure. We allowed for a 10-minute relaxation after reaching our desired pressure; further relaxation during measurement is found to decrease exponentially<sup>59</sup>. The pressure drift uncertainty,  $\delta_{\Delta P}$ , was modeled as half the difference between the pressures measured before and after the Brillouin scattering scan.

$$\delta_{\Delta P} = \frac{P_{before} - P_{after}}{2} \quad (18)$$

The relaxation typically was on the order of 0.1 GPa over 10 minutes. There were a few points that had a larger uncertainty for measurements taken over night, where the relaxation could be as high as 0.2 GPa.

A final source of pressure uncertainty could arise from laser-induced heating of the ruby. A drawback of using ruby as a pressure calibrant is that both pressure and temperature cause a redshift in the fluorescence, suggesting a higher than actual pressure [32]. To obtain an accurate reference R<sub>1</sub> wavelength, an identical ruby to that used in our experiments was placed in an empty gasket at ambient pressure. The R<sub>1</sub> ruby wavelength was measured as a function of laser power starting at 100 mW and extrapolated back to 0 mW. We found that the change in the R<sub>1</sub> wavelength with respect to power varied over 1 mW as  $\Delta\lambda = -4.15 \times 10^{-3} \text{ nm}$ . Alternatively, one degree of heating would give a R<sub>1</sub> wavelength shift of  $\Delta\lambda \cong +7.4 \times 10^{-3} \text{ nm}$ <sup>40</sup>. Were the shift in the R<sub>1</sub> line only due to heating effects from the laser, our data would indicate that the laser-cooled the ruby by half a degree at 100mW. We take this to mean that the reference rubies were not heated to a physically significant extent.

We calculate the uncertainty in pressure using Gaussian quadrature, as given by

$$\sigma_P = \sqrt{(\delta_{\Delta P})^2 + (\delta_{P_{inst}})^2} \quad (19)$$

The primary source of experimental uncertainty in the density arises from uncertainties in the alignment of the DAC and the Brillouin scattering geometry; small errors in the setup will have a noticeable effect on the Brillouin shift and the resulting sound velocity. Quantification of possible sources of error in sound velocity measurements obtained from Brillouin scattering in DACs has been outlined in detail previously<sup>60-62</sup>. To Summarize, there are four main possible

sources of error in the setup of the DAC and the alignment of the Brillouin system for a fluid sample.

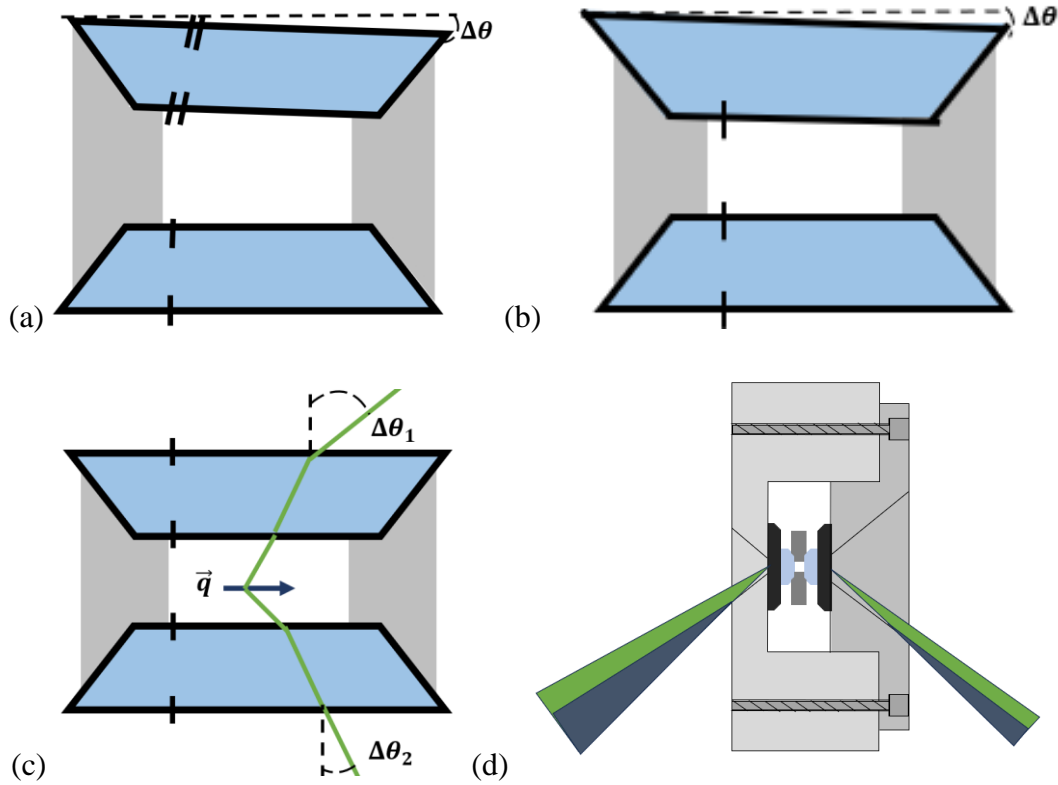


**FIG. 12** An outline of possible errors in DAC alignment and setup. (a) Two parallel-cut diamonds are not parallel with respect to one another. (b) A diamond whose back plate is not parallel to its culet. (c) The incident angle is different from the scattered angle. (d) Vignetting of the beam by the DAC. Single and double dashed lines along the diamond interfaces indicate parallelism. All examples are exaggerated relative to what one would expect in a real experiment.

The first alignment error that may occur is vignetting (Fig. 8d), where the laser is clipped or obstructed by the experimental setup. This will not occur with a well-focused laser with this experiment's  $90^\circ$  DAC seat openings in the  $50^\circ$  scattering geometry used in the Brillouin measurement. Asymmetric scattering angles (Fig. 8c) produce an error in velocity of approximately 0.01% for every  $1^\circ$  error<sup>61</sup>. Figures 8a and 8b provide most of the error in the measured Brillouin scattering shift. Further, both of these provide a symmetric error measurement, allowing one to measure the sample twice, one turned  $180^\circ$ , and averaging the measured velocities to obtain the true velocity. This method was tested multiple times over the course of the experiment giving a difference between 20-60 m/s, amounting to approximately a 0.4% error in velocity based on pressure. Another source of experimental uncertainty came from the resolution of the angle used, which was reported to one decimal point, providing a  $\pm 0.04^\circ$  uncertainty in the nominal value for the scattering angle. This corresponds to an uncertainty, based on the scattering angle, of 0.3%. Both the experimental uncertainty and resolution of the scattering angle provide an upper limit of 0.7% of the error in the velocity.

Another source of  $\rho$  uncertainty we considered is that associated with temperature. The reported room temperatures in previous  $H_2$  and He experiments range from 293 K to 300 K. P-V-T EOS

developed for H<sub>2</sub><sup>22, 33</sup> and He<sup>34</sup> indicate very little deviation across this temperature range. Matsuishi *et al.* indicate a maximum temperature difference of 0.617% at 0.5 GPa and a minimum difference of 0.038% at 5.4 GPa. Mills *et al.* H<sub>2</sub> similarly indicates a difference in density between 293 K and 300 K of 0.62% over the same pressure range. Mills *et al.* He P-V-T EOS indicates a maximum temperature-dependent difference of density of 0.869% at 0.5 GPa and a minimum of 0.415% at 2 GPa. Extrapolating Mills's He results to 5.4 GPa, the temperature-dependent difference in density is 0.269%. These deviations from the  $\rho$ -P EOS are within the desired accuracy of 1%. The acceptable tolerance of the density with respect to temperature will allow us to use the average temperature of this range of 296 K without loss of the accuracy we seek. This temperature is also consistent with temperature of 24-hour periods over which the measurements were taken at Brillouin scattering hutch at 296(+/-1) K.

The main density uncertainty comes from the uncertainty in pressure over the range of numerical integration, which arises due to the assumption of constant density over the interval of integration. This error is roughly on the same order of magnitude as the error in density associated with the uncertainty in velocity. Using Gaussian quadrature again, the uncertainty in density is given by:

$$\sigma_{\rho} = \sqrt{\left(\frac{\partial \rho}{\partial U_l} \delta_{\rho U_l}\right)^2 + \left(\frac{\partial \rho}{\partial P} \delta_P\right)^2} \quad (20)$$